ADVANCED MATERIALS TECHNOLOGIES
www.advmattechnol.de

Selective Ion Detection with Integrated Organic Electrochemical Transistors

*Dimitrios A. Koutsouras, Katharina Lieberth, Fabrizio Torricelli, Paschalis Gkoupidenis, and Paul W. M. Blom**

Accurate sensing of ion concentrations in body fluids is of importance to monitor cell functions, and any deviation of the concentration serves as a warning sign of pathophysiological conditions. Here, a fabrication approach for an integrated device consisting of two electrochemical transistors, capable of selective simultaneous detection between potassium and sodium ions in an analyte is demonstrated. A common in-plane gate electrode is integrated in the substrate, enabling the fabrication of micro-scale ion sensors for biomedical applications. The approach is versatile and can be extended to include numerous ion-selective transistors on a chip in order to meet the demand for simultaneous sensing of multiple ions.

1. Introduction

Electrolytes play an important role in biology as they are indispensable in a variety of physiological processes. They are salts which, when dissolved in polar solvents such as water, are separated into anions and cations and produce conducting solutions. They are responsible for the proper functioning of cells by regulating their osmotic pressure, they assist the creation and propagation of electrical signals in neural and muscle cells, and they facilitate the release of hormones from endocrine glands. In particular, they create osmotic gradients between the extracellular and intracellular environments, which control the biological tissue hydration, the blood pH and support organ functions. Deviation of the concentration of these species from the normal ranges in the body fluids is an indication of diseases such as diabetes, liver and renal dysfunctions, and cardiovascular physiological disorders.[1,2] Especially sodium (Na^+) and potassium (K^+) are a "dynamic duo" that is responsible for the blood pressure regulation, the transmission of nerve signals in electrogenic cells and for the muscle contraction.[3,4] Therefore, there is an imperative need for precise and reliable ion-sensing devices for a real-time and accurate monitoring of ion concentrations in electrolytes. These devices find numerous applications in multiple fields like in healthcare diagnostics, in the pharmaceutical industry, and in food and water security testing.[5]

The most studied device for ion detection is the ion-sensitive field-effect transistor (ISFET). The ISFET architecture is based on a conventional field-effect transistor structure where an electrolyte solution is placed between the gate (named reference electrode) and the insulator.[6–8] ISFETs were based on the silicon technology where a direct contact between the electrolyte and the channel is not possible. More recently, using emerging technologies based on metal oxides, graphene and organic conductors the ISFET architecture has been further developed by removing the insulating layer.[9–11] The direct contact between the electrolyte solution and the semiconducting channel results in both lower operating voltage and improved sensitivity. Among the various technological approaches, organics have gained significant attention due to their comparative advantages. Organics can be processed at low temperature, are soft resulting in a mechanical compatibility with biological tissues, support mixed ionic-electronic conductivity, and their properties can be chemically-tuned for targeting specific application requirements. Focusing on bioelectronic applications, other essential features offered by organics are the stability in aqueous environment and, when used in a transistor architecture, device operation well below 1 V has been demonstrated.[11–16] The latter characteristic is important to avoid electrolysis.

In electrolyte-gated organic transistors the transistor's channel is in contact with the gate through the electrolyte.[17] In this configuration, the organic channel material can be either impermeable or permeable to the ions of the electrolyte. In the former mode of operation, a nanometric thick "electrical double layer" (EDL) is formed both at the gate/electrolyte and the electrolyte/channel interface. The electrolyte/channel EDL provides capacitance values in the order of $\approx 1 \div 10\ \mu F cm^{-2}$, which results in a sub-volt voltage operation.[18,19] In the latter mode of operation the organic semiconductor is permeable to the electrolyte, giving rise to the class of organic electrochemical transistors (OECTs).[20] Since the whole volume of the film participates in

D. A. Koutsouras, K. Lieberth, P. Gkoupidenis, P. W. M. Blom
Max Planck Institute for Polymer Research
Ackermannweg 10, Mainz 55128, Germany
E-mail: blom@mpip-mainz.mpg.de
F. Torricelli
Department of Information Engineering
University of Brescia
Via Branze 38, Brescia 25123, Italy

The ORCID identification number(s) for the author(s) of this article can be found under https://doi.org/10.1002/admt.202100591.

DOI: 10.1002/admt.202100591

the process,[21] a volumetric capacitance is displayed and, as a result, OECTs can provide a very large transconductance (in the mS range). Hence, OECTs are very useful in transducing signals of biological origin.[22–26] OECTs typically use the conducting polymer poly(3,4-ethylenedioxythiophene) polystyrene sulfonate (PEDOT:PSS) and the large hole concentration in the polymer results in a depletion mode of operation.

Due to their ability to convert ionic into electrical signals, OECTs have recently been used for the development of enhanced ion-detection and real-time monitoring.[27–31] These devices show selective detection of various ions, low detection limit and small response times. However, they typically use a suspended Ag/AgCl electrode as gate which is immersed in the electrolyte on top of the devices, hindering integration and further device miniaturization. Here, we demonstrate an integrated ion-selective device based on OECTs using a PEDOT:PSS gate electrode in an in-plane configuration. The gate geometry was tuned in order to gate the transistor channels similarly to a Ag/AgCl gate. On the same substrate, two groups of different ion-selective transistors where fabricated, a potassium-selective and a sodium-selective one, realizing a simultaneous ion-selective functionality with the use of a single in-plane gate. This work is a step forward toward multifunctional bioelectronic ion-selective biochips in a monolithic configuration.

2. Results and Discussion

The device architecture is schematically presented in **Figure 1**a. The OECT channel and the in-plane gate were fabricated with standard microfabrication techniques. Shortly, a photolithography step defined the source, drain, and (in-plane) gate electrodes on an optical microscope glass slide that served as a substrate. Two layers of parylene C were used to electrically insulate the device, while a reactive ion etching process opened windows in the parylene C at predetermined points of interest. These openings were subsequently filled with PEDOT:PSS, creating the device gate and channel through a peel-off step of the second (sacrificial) parylene C layer, which patterned the conducting polymer. The gate electrode was designed with an area much larger than the channel area of the transistor, allowing for an efficient gating of the channel.[32] The selectivity for ion sensing is based on the presence of ion-selective membranes (ISMs) that are deployed between the analyte and the recording site.[33,34] These ISMs consist of a plasticized poly(vinyl chloride) (PVC) matrix that incorporates ionophores that selectively and reversibly interact with the target ions (primary ions) and form complexes. They also incorporate ionic sites that prevent counter ions from the solution to enter the membrane via the Donnan exclusion effect and promote the exchange of the primary ions.[34] Theoretically, changes in the concentration of the primary ion in the analyte induces a potential difference at the ISM interface that modulates the drain current (I_{ds}) of the transistor. Nevertheless, the low mobility of the ions in the PVC matrix renders their transport problematic and has a severe effect on the device performance. One approach to address this issue is by an increase of the ionic sites as already been proposed.[30] There is, though, a range, to the ionophores, molar ratios (0.2–0.8) outside of which the free vacant ionophores in the membrane are depleted. As a consequence, the selectivity and the sensitivity of the ISM deteriorates since the formation of ion-ionophore complexes is devastated.[28] An alternative approach is the use of an internal electrolyte "reservoir," which is typically placed between the ISM and the channel to supply enough ions for sufficient channel gating. In previous works, liquid or hydrogel electrolytes where used which dictates, though, the use of a well (typically made of glass or polydimethylsiloxane (PDMS)).[27] This makes the miniaturization of the device rather problematic. Recently, a thin polyelectrolyte film with mobile sodium ions (polyelectrolyte poly(sodium4-styrenesulfonate- PSSNa) as the internal reservoir was used, facilitating easier device miniaturization.[28] We therefore adopted this approach of using a PSSNa film as ion reservoir in order to achieve an integrated sensing device. However, we note that in their approach Han et al. used an Ag/AgCl gate electrode, which is typically employed in OECT applications due to its faradaic mode of operation. Such a hovering Ag/AgCl electrode is not compatible with efficient management of space in biosensing microchips. Our approach replaces the hovering Ag/AgCl electrode with a planar PEDOT: PSS in-plane gate. The gate area is chosen to be larger than then channel area so that it results in a polarizable mode of operation, with the advantage

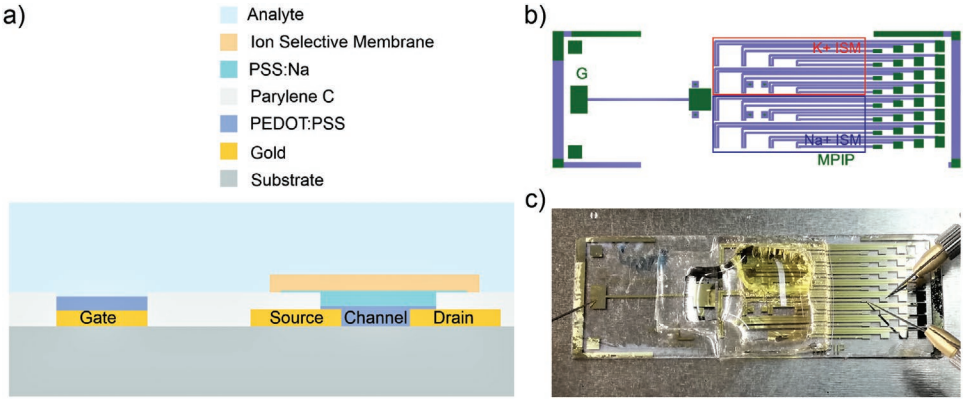

Figure 1. a) Schematic representation of the ISM-OECT cross section (not in scale). b) Top view of the device layout. A 16 (4 × 4) multi-channel grid is gated by a common gate electrode. Half of the channels are coated with a K^+-ISM while the other half are coated with a Na^+-ISM, creating a multifunctional device able to sense simultaneously both ions. c) An optical micrograph of the device. The analyte overflows the compartments establishing a connection between the gate and the ISM-OECT channels.

of the monolithic incorporation of every chip element in the same plane. In addition, the use of PDMS compartments in our work allows for the incorporation of multiple different ISMs which serve as a proof of concept of the advantage of a targeted functionalization of every single channel on the same substrate.

In our fabrication approach, PSSNa was drop casted on top of the channels followed by a drop casting of the ISM. The addition of the analyte establishes a physical connection between the planar gate and the channel, creating a stack consisting of film layers (PEDOT:PSS, PSSNa, and ISM), the liquid electrolyte and the gate electrode in a "planar sandwich" configuration. Detailed information regarding the fabrication process is provided in the experimental section.

The device was designed to integrate multiple channels all of which are gated by a single in-plane gate. Half of the channels were covered with a potassium-selective membrane and the other half with a sodium-selective one (Figure 1b). This layout allows for a selective distinction between K^+ and Na^+ by enabling the sensing system to simultaneously sense the presence of various ions in the same solution. Special attention was devoted to avoid any cross talk between the K^+-ISM and Na^+-ISM deposited on the OECTs. For that, a PDMS well was used to create separate compartments for the K^+- and Na^+- selective transistors. The well was attached on the substrate with the help of a small amount of PDMS, which after an overnight drying process created a watertight partitioning. In one compartment the K^+-ISM mixture was drop-casted and left to dry over night while the Na^+-ISM mixture was drop-casted and dried in the other. A third compartment was reserved for the in-plane gate. The used electrolyte (analyte) in every compartment was left to overflow, thus creating a connection between all of them. Therefore, the gate was able to modulate the current in each transistor via the electrolyte solution and through the ISM and the PSSNa films (Figure 1c).

For the potassium-selective OECT sensor, a 50 µm x 50 µm (width x length) PEDOT: PSS channel with thickness of 100 nm was employed. The ISM on it was doped with potassium ionophores. The output curves of the devices in a 0.1 M KCl solution are displayed in **Figure 2**a. The gate voltage sweeps from V_{gs} = –0.6 V to V_{gs} = +1 V and the source-drain current I_{ds} is recorded as a function of the applied source drain voltage V_{ds} with a step of 0.05 V. The transfer curve and the transconductance (g_m) of the device in the same solution are shown in Figure 2b. The device exhibits a transconductance of around 1.5 mS, which is typical for an OECT of this geometry. Despite the fact that the fabrication process involves multiple film deposition steps and the gate is placed on the same plane as the channel in an unorthodox "planar sandwich" set up, typical drain-current modulation is obtained. The efficient channel gating is achieved by proper sizing the gate geometry and material. More in detail, the PEDOT:PSS thickness on the gate is 100 nm and the electrode size is 4000 µm x 4000 µm.

The situation is similar for the sodium-selective OECT device. A 50 µm x 50 µm PEDOT:PSS channel with a thickness

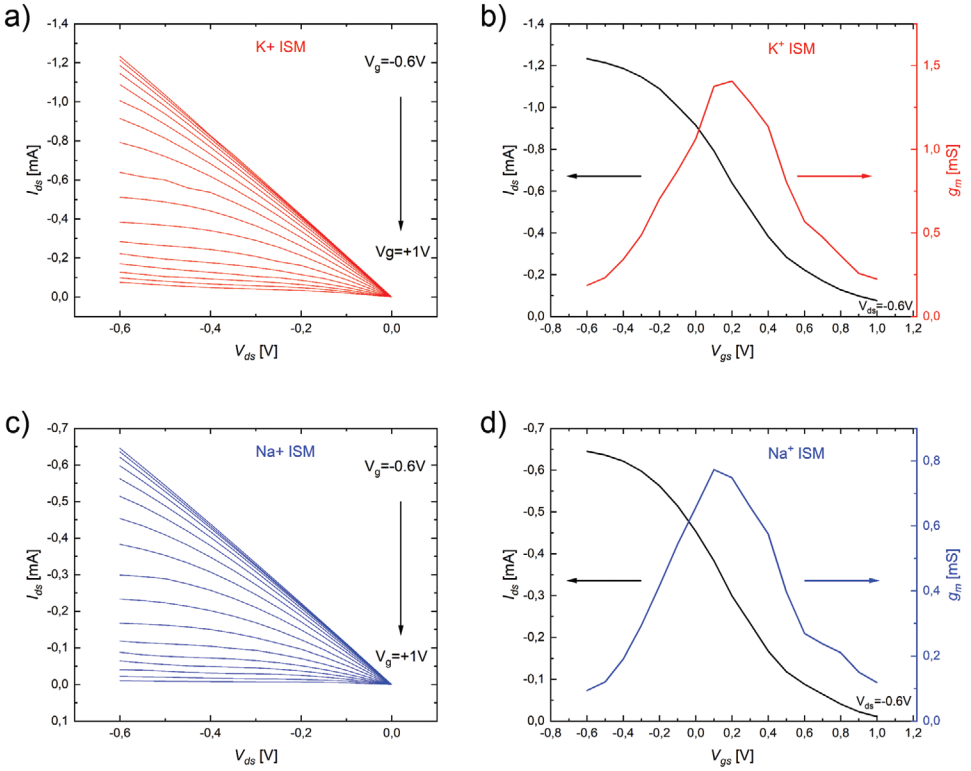

Figure 2. ISM OECT electrical characteristics. a) Output curves of the K^+-ISM OECT in KCl 0.1 M. The gate voltage sweeps from V_{gs} = –0.6 V to V_{gs} = +1 V. b) Transfer curve and the corresponding transconductance of the same device at a source drain bias of V_{ds} = –0.6 V. c) Output curves of the Na^+-ISM OECT in NaCl 0.1 M. The gate voltage sweeps from V_{gs} = –0.6 V to V_{gs} = +1 V. d) Transfer curve and the corresponding transconductance of the same device at a source drain bias of V_{ds} = –0.6 V.

of 100 nm is gated by the same gate electrode on the same substrate. The sodium ionophores doped ISM renders the device sensitive to Na^+ which is now the primary ion. Figure 2c presents the output curves of the Na^+-selective OECT. Again, the gate bias is swept from V_{gs} = –0.6 V to V_{gs} = +1 V and I_{ds} is recorded as a function of V_{ds}. Now, the used electrolyte is 0.1 M NaCl. The corresponding transfer curve is shown in Figure 2d delivering a transconductance value of around 0.8 mS.

After the independent electrical characterization of the ion-selective devices, their response to different analyte concentrations was tested simultaneously. In general, the channel current depends both on the sign and magnitude of the applied gate voltage as well as on the ion concentration in the electrolyte. Focusing on the electrical transfer characteristics, the I_{ds}–V_{gs} curves shifts to less positive voltages when the ion concentration increases.[28,35] More in detail, an increase in the primary ion concentration results in an increase of the potential between the analyte and the ion selective membrane. Consequently, for a given V_{gs} an increased number of Na^+ from the PSSNa layer will be injected into the PEDOT:PSS film and the channel current will be reduced. According to these considerations, we investigated the impact of different ionic solutions on the K^+- and Na^+- selective OECT devices by measuring the I_{ds}–V_{gs} characteristics at various ion concentrations and types. The concentration of NaCl was increased stepwise, by a factor of 10 in each step, from 10^{-7} to 10^{-3} M. **Figure 3** presents the resulting transfer curves.

In the case of the potassium-selective device the presence of the NaCl solution (interfering ion) has a less intense effect on the channel current compared to the effect of a KCl solution (primary ion) of the same concentration. In fact, for concentrations up to 10^{-4} M NaCl (blue curves in Figure S1, Supporting Information) there is not significant device response as a function of the interfering ion concentration. Even for the largest NaCl concentrations an overlap occurs only with the smallest KCl concentrations which are orders of magnitude lower. Figure 3a reports mean drain current values obtained from 3 different measurements on the same device. Each individual measurement is shown in Figure S1, Supporting Information. The error bars represent the standard deviation of the measured data. On the contrary, for KCl solutions (red curves in Figure 3a) the de-doping effect is much more pronounced for the same range of concentrations. In addition, each increase in the KCl solution concentration is echoed in the plot by a greater decrease in the channel current due to the more extent channel de-doping. To sum up, the same device responds differently for the analyte that bares the primary ion (K^+) compared to the one that bares the interfering one (Na^+) for any given electrolyte concentration. The de-doping effect in the channel is more pronounced when KCl is used compared to NaCl, a fact that demonstrates the ability of the device to distinguish between the two ions.

The situation is reversed for the sodium-selective OECT. Figure 3b reports the transfer curves for this device. Again, the drain current values are mean values of 3 consecutive measurements (each shown in Figure S1, Supporting Information). In red, the channel response is shown when a KCl solution (interfering ion) was used as the electrolyte. The analyte concentration was increased stepwise from 10^{-7} to 10^{-3} M. For every concentration up to 10^{-4} M (Figure S1, Supporting Information) the channel is less de-doped compared to the de-doping induced by a solution of the same concentration of the primary ion. Even for the maximum concentration that was used for the interfering ion (KCl 10^{-3} M) the de-doping is comparable to the one achieved with the minimum NaCl concentrations despite the fact that the latter are orders of magnitude smaller. In contrast, when the primary ion solution is used, namely NaCl, the channel de-doping is more pronounced, compared to KCl, for the same concentration range. Again, the increase of the NaCl concentration results in a greater decrease in the recorded current due to de-doping. In addition, Figure S2, Supporting Information, reports the source drain current I_{ds} versus the analyte concentration at V_g = 0.2 V for the ISM devices of Figure 3. For the same applied gate voltage, the de-doping is always more pronounced for the primary ion on each ISM resulting in a lower channel current. Therefore, on the same substrate two device flavors are integrated, one more sensitive to the presence of K^+ and the other more sensitive to the presence of Na^+ in the analyte. The experiments were repeated on a newly fabricated set of devices (Figure S3, Supporting Information) and identical results were obtained, demonstrating the reproducibility of the integrated ISM devices. The stability of both the K^+ ISM and the Na^+ ISM was also tested. Figure S4, Supporting Information,

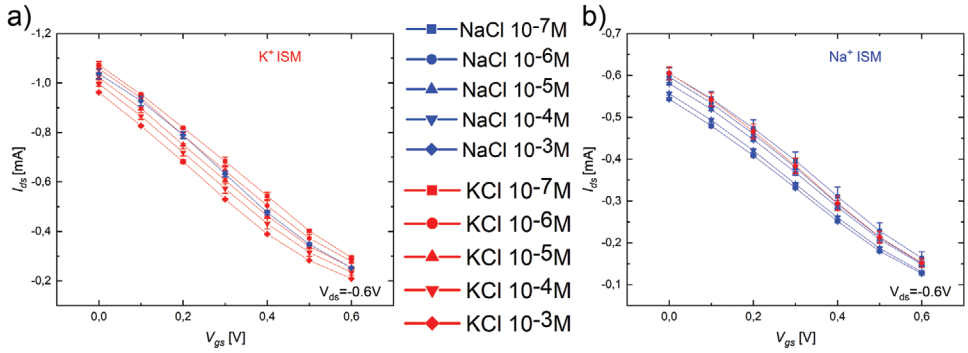

Figure 3. Transfer curves of the ISM-OECTs for different analyte concentrations. a) K^+-ISM OECT. As expected, for the same concentrations, the gating effect is more pronounced when KCl (in red) is used compared to NaCl (in blue). Therefore, the device can distinguish between the two ions. b) Na^+-ISM OECT. Now, the primary ion Na^+ (in blue) causes a larger de-doping of the channel compared to the interfering ion K^+ (in red). Every transfer curve was obtained at V_{ds} = –0.6 V. Both plots show the mean drain current values of 3 consecutive measurements and the error bars report the standard deviation of the data. For clarity reasons only the maximum concentration of the interfering ion (concentration equal to 10^{-3} M) is plotted.

shows various transfer characteristics and the drain current versus time curves. In the case of K^+ selective OECTs a shift of the transfer characteristics as low as 0.04 V is displayed while in the case of Na^+ selective OECTs the transfer characteristics are almost perfectly overlapped. As a further confirmation of the device stability, the drain current at $V_g = 0$ V and $V_{ds} = -0.2$ V is measured as a function of time. Figure S4b,d, Supporting Information, show that I_{ds} is perfectly stable over 25 min of continuous device biasing. Finally, the real-time response of the ISM devices when the analyte concentration was varied stepwise is presented in Figure S5, Supporting Information. The measurements show the device operation when the concentration of K+ (Figure S5a, Supporting Information) and Na+ (Figure S5b, Supporting Information) ranges from 10^{-7} to 10^{-3} M and the time response is of the order of few tens of seconds.

3. Conclusion

In conclusion, based on the advantages that OECTs offer for accurate and precise ion-selective sensors, we demonstrate a fabrication approach that allows for the integration of two different ion-selective devices on the same substrate. The OECT gate is also integrated in the substrate, in a relatively unexplored architecture for ISM sensors, realizing an integrated multifunctional sensor for biomedical and pharmaceutical applications. The proposed approach is versatile and allows for integration of numerous ion-selective OECTs on the same substrate in order to successfully meet any demand for multiple ion sensing.

4. Experimental Section

Materials: PEDOT:PSS (Clevios PH1000), Soap (Micro-90), poly(sodium4-styrene sulfonate) (PSSNa), ethylene glycol, 4-dodecylbenzenesufonic acid (DBSA), PDMS, and 3-methacryloxypropyltrimethoxysilane (GOPS) (Sigma-Aldrich).

PEDOT:PSS Formulation: 2 mL of ethylene glycol (conductivity enhancement), 50 µL of DBSA (film formation) and 0.4 mL of GOPS (surface adhesion promoter and polymer cross-linker agent) in 38 ml of PEDOT:PSS.

PSSNa Mixture: 1.2% w/v aqueous PSSNa solution with DBSA (0.25% v/v), GOPS (1% v/v), and 1 M HCl (1% v/v). HCl was added in order to enhance the crosslinking reaction through pH modification.[28]

K^+-Ion-Selective Membrane: High molecular weight PVC (36.5 wt%), potassium Ionophore III (2.5 wt%), potassium tetrakis(4-chlorophenyl-) borate (0.5 wt%), and diisodecyl adipate (60.5 wt%) in THF (500 mg/5 mL).[29]

Na^+-Ion-Selective Membrane: High molecular weight PVC (26.8 wt%), sodium Ionophore X (6.5 wt%), 2-nitrophenyl octyl ether (66.7 wt%) in THF (770 mg/11.7 mL).

The ISM mixture was drop casted on the OECT channels and was left to dry overnight. Different PDMS compartments were used to separate the two ISMs.

Device Fabrication: The devices were fabricated using standard microfabrication techniques. 26 mm x 76 mm optical microscope glass slides were thoroughly cleaned successively in a soap (1% vol vol^{-1}, Micro-90) and an acetone/isopropanol (1:1 solvent mixture) sonication bath. Initially, a first photolithography step (used photoresist: S1813) and a following sputtering gold deposition step defined the source, drain, and gate electrodes on the substrate (Pfeiffer-vacuum sputtering system). The gold electrode thickness was 100 nm while a 5 nm chromium layer was used to promote adhesion of the electrodes on the substrate. The devices were, then, encapsulated in a double, 2 µm each in thickness, parylene C layer. The first parylene C layer was firmly attached on the substrate with the help of Silane A-174 (gamma-methacryloxypropyltrimethoxysilane) which was used as adhesion promoter. In contrast, the second parylene C layer was deposited after soap solution (1% vol vol^{-1} in distilled water, Micro-90) was spin coated on the first layer. The purpose of that was the facilitation of the lift-off process in a subsequent fabrication phase. A second photolithography step followed (used photoresist: AZ 9260) in order for windows in the photoresist in predefined spots above the common gate electrode and the transistors' channels to be created. Reactive ion etching with O_2/CF_4 plasma was used to remove parylene C under these windows and to expose the gold electrodes and the transistors' channels. PEDOT:PSS was spin-coated on the chip and a final peel-off step defined both the channel of the OECT and the common gate. The devices were, then, hard baked for an hour at 140 °C and placed in distilled water over night for the removal of the excess of low molecular weight molecules from PEDOT:PSS. A PDMS well with 3 separate compartments was then glued on the chip separating the channels that serve as potassium-selective sensors from the channels that serve as sodium-selective sensors and from the common gate. The PSSNa mixture was drop casted in the transistors compartment but not in the gate compartment and it was baked at 130 °C for 1 h for the polyelectrolyte to be crosslinked.[28] After an overnight immersion in 0.1 M NaCl solution for the removal of any excess compounds and the conservation of Na^+, PSSNa was ready to serve as the inner electrolyte "reservoir" during the operation of the device.[28] Next, inside the potassium-selective compartment of the chip the potassium ISM mixture was drop casted on top of the PSSNa film while inside the sodium-selective compartment of the chip the sodium ISM mixture was drop casted on top of the PSSNa film. After an overnight drying process in room temperature both ISMs were successfully formed.

Device Characterization and Measurements: The transistors were characterized and the measurements were performed with a dual channel Keithley 2600 SMU.

Supporting Information

Supporting Information is available from the Wiley Online Library or from the author.

Acknowledgements

Open access funding enabled and organized by Projekt DEAL.

Conflict of Interest

The authors declare no conflict of interest.

Data Availability Statement

The data that support the findings of this study are available from the corresponding author upon reasonable request.

Keywords

in-plane gating, ion selective devices, ion selective membranes, organic electrochemical transistors

Received: July 6, 2021
Published online:

[1] Q. J. Wan, P. Kubáň, J. Tanyanyiwa, A. Rainelli, P. C. Hauser, *Anal. Chim. Acta* **2004**, *525*, 11.
[2] F. Ghaderinezhad, H. C. Koydemir, D. Tseng, D. Karinca, K. Liang, A. Ozcan, S. Tasoglu, *Sci. Rep.* **2020**, *10*, 13620.
[3] K. J. Aaron, P. W. Sanders, *Mayo Clin. Proc.* **2013**, *88*, 987.
[4] S. Kaushik, R. Kumar, P. Kain, *J. Exp. Neurosci.* **2018**, *12*, 117906951880689.
[5] C. Jimenez-Jorquera, J. Orozco, A. Baldi, *Sensors* **2010**, *10*, 61.
[6] P. Bergveld, *Sens. Actuators, B* **2003**, *88*, 1.
[7] M. Spijkman, E. C. P. Smits, J. F. M. Cillessen, F. Biscarini, P. W. M. Blom, D. M. de Leeuw, *Appl. Phys. Lett.* **2011**, *98*, 043502.
[8] P. Bergveld, *IEEE Trans. Biomed. Eng.* **1970**, *70*, BME-17.
[9] M.-J. Spijkman, J. J. Brondijk, T. C. T. Geuns, E. C. P. Smits, T. Cramer, F. Zerbetto, P. Stoliar, F. Biscarini, P. W. M. Blom, D. M. de Leeuw, *Adv. Funct. Mater.* **2010**, *20*, 898.
[10] W. Fu, C. Nef, A. Tarasov, M. Wipf, R. Stoop, O. Knopfmacher, M. Weiss, M. Calame, C. Schönenberger, *Nanoscale* **2013**, *5*, 12104.
[11] J. T. Mabeck, G. G. Malliaras, *Anal. Bioanal. Chem.* **2006**, *384*, 343.
[12] D. A. Koutsouras, A. Hama, J. Pas, P. Gkoupidenis, B. Hivert, C. Faivre-Sarrailh, E. Di Pasquale, R. M. Owens, G. G. Malliaras, *MRS Commun.* **2017**, *7*, 259.
[13] J. Rivnay, R. M. Owens, G. G. Malliaras, *Chem. Mater.* **2014**, *26*, 679.
[14] T. Someya, Z. Bao, G. G. Malliaras, *Nature* **2016**, *540*, 379.
[15] D. A. Koutsouras, R. Perrier, A. V. Marquez, A. Pirog, E. Pedraza, E. Cloutet, S. Renaud, M. Raoux, G. G. Malliaras, J. Lang, *Mater. Sci. Eng., C* **2017**, *81*, 84.
[16] D. Khodagholy, T. Doublet, P. Quilichini, M. Gurfinkel, P. Leleux, A. Ghestem, E. Ismailova, T. Hervé, S. Sanaur, C. Bernard, G. G. Malliaras, *Nat. Commun.* **2013**, *4*, 1575.
[17] S. H. Kim, K. Hong, W. Xie, K. H. Lee, S. Zhang, T. P. Lodge, C. D. Frisbie, *Adv. Mater.* **2013**, *25*, 1822.
[18] L. Kergoat, L. Herlogsson, D. Braga, B. Piro, M.-C. Pham, X. Crispin, M. Berggren, G. Horowitz, *Adv. Mater.* **2010**, *22*, 2565.
[19] F. Buth, D. Kumar, M. Stutzmann, J. A. Garrido, *Appl. Phys. Lett.* **2011**, *98*, 153302.
[20] H. S. White, G. P. Kittlesen, M. S. Wrighton, *J. Am. Chem. Soc.* **1984**, *106*, 5375.
[21] D. A. Bernards, G. G. Malliaras, *Adv. Funct. Mater.* **2007**, *17*, 3538.
[22] J. Rivnay, P. Leleux, M. Ferro, M. Sessolo, A. Williamson, D. A. Koutsouras, D. Khodagholy, M. Ramuz, X. Strakosas, R. M. Owens, C. Benar, J.-M. Badier, C. Bernard, G. G. Malliaras, *Sci. Adv.* **2015**, *1*, e1400251.
[23] D. A. Koutsouras, P. Leleux, M. Ramuz, J. Rivnay, G. G. Malliaras, in *2014 IEEE International Electron Devices Meeting* **2014**, pp. 31.4.1–31.4.4.
[24] P. Lin, F. Yan, *Adv. Mater.* **2012**, *24*, 34.
[25] D. Khodagholy, J. Rivnay, M. Sessolo, M. Gurfinkel, P. Leleux, L. H. Jimison, E. Stavrinidou, T. Herve, S. Sanaur, R. M. Owens, G. G. Malliaras, *Nat. Commun.* **2013**, *4*, 2133.
[26] D. Khodagholy, J. N. Gelinas, Z. Zhao, M. Yeh, M. Long, J. D. Greenlee, W. Doyle, O. Devinsky, G. Buzsáki, *Sci. Adv.* **2016**, *2*, e1601027.
[27] M. Sessolo, J. Rivnay, E. Bandiello, G. G. Malliaras, H. J. Bolink, *Adv. Mater.* **2014**, *26*, 4803.
[28] S. Han, S. Yamamoto, A. G. Polyravas, G. G. Malliaras, *Adv. Mater.* **2020**, *32*, 2004790.
[29] M. Ghittorelli, L. Lingstedt, P. Romele, N. I. Crăciun, Z. M. Kovács-Vajna, P. W. M. Blom, F. Torricelli, *Nat. Commun.* **2018**, *9*, 1441.
[30] S. T. Keene, D. Fogarty, R. Cooke, C. D. Casadevall, A. Salleo, O. Parlak, *Adv. Healthcare Mater.* **2019**, *8*, 1901321.
[31] P. Romele, P. Gkoupidenis, D. A. Koutsouras, K. Lieberth, Z. M. Kovács-Vajna, P. W. M. Blom, F. Torricelli, *Nat. Commun.* **2020**, *11*, 3743.
[32] F. Cicoira, M. Sessolo, O. Yaghmazadeh, J. A. DeFranco, S. Y. Yang, G. G. Malliaras, *Adv. Mater.* **2010**, *22*, 1012.
[33] A. Cadogan, Z. Gao, A. Lewenstam, A. Ivaska, D. Diamond, *Anal. Chem.* **1992**, *64*, 2496.
[34] C. Bieg, K. Fuchsberger, M. Stelzle, *Anal. Bioanal. Chem.* **2017**, *409*, 45.
[35] G. Tarabella, C. Santato, S. Y. Yang, S. Iannotta, G. G. Malliaras, F. Cicoira, *Appl. Phys. Lett.* **2010**, *97*, 123304.